Optical Materials 104 (2020) 109847

Contents lists available at ScienceDirect

Optical Materials

journal homepage: http://www.elsevier.com/locate/optmat

Scintillation, luminescence and optical properties of Ce-Doped borosilicate glasses

Linyu Pan [a], Juliana K.M.F. Daguano [b,c], Neilo M. Trindade [a,d,f], Mayara Cerruti [b], Edgar D. Zanotto [b], Luiz G. Jacobsohn [a,e,*]

[a] Department of Materials Science and Engineering, Clemson University, Clemson, SC, USA
[b] Department of Materials Engineering, Federal University of São Carlos, São Carlos, SP, Brazil
[c] Center for Engineering, Modeling and Applied Social Sciences, Federal University of ABC, Santo André, SP, Brazil
[d] Department of Physics, Federal Institute of Education, Science and Technology of São Paulo, São Paulo, SP, Brazil
[e] Center for Nuclear Environmental Engineering Sciences and Radioactive Waste Management (NEESRWM), Clemson University, Anderson, SC, USA
[f] Institute of Physics, University of São Paulo - USP, São Paulo, SP, Brazil

ARTICLE INFO

Keywords:
Borosilicate glass
Cerium doping
Luminescence
Thermoluminescence
Scintillator

ABSTRACT

The structure, ultraviolet (UV) transparency, luminescence, and scintillation of CeO_2-doped (0.1 mol%) borosilicate glasses containing Sb_2O_3, SnO_2 or P_2O_5 were investigated. Glasses were prepared by melt quenching in air and characterized by several spectroscopy techniques: Raman scattering, optical absorption, photoluminescence (PL), fluorescence lifetime, thermoluminescence, and radioluminescence. Raman scattering results presented three major groups of vibrational modes, within 230–850 cm^{-1}, 850-1250 cm^{-1}, and 1250-1600 cm^{-1}. Luminescence was dominated by a broad band centered at around 360–380 nm, depending on the chemical composition of the glass. Photoluminescence presented a dominant (96–98%) fast decay time of 36–40 ns that was ascribed to Ce^{3+}. The P_2O_5-containing glass showed the highest scintillation output under X-ray excitation.

1. Introduction

Scintillators are materials capable of emitting luminescence due to exposure to ionizing radiation, and find application in several fields, *e.g.*, medical imaging, homeland security, high energy physics, and oil exploration [1–7]. Scintillators are fabricated in many forms, including single crystals, polycrystalline ceramics, and glasses. Glass scintillators are particularly attractive due to advantages over single crystals and transparent polycrystalline ceramics such as low-cost, fast, and large area/volume production, and nearly limitless options for chemical composition. Rare earth ions are normally adopted as luminescence activators in scintillating glasses, with Ce^{3+} being the most common because of its fast allowed $5d \rightarrow 4f$ transition. However, the luminescence of Ce^{3+} is strongly influenced by the chemical composition and atomic arrangement of the nearest neighbors [8–12]. Therefore, investigation of the luminescence of Ce^{3+} in different glasses is an active research topic [13–20]. In this work, an exploratory investigation on the effects of the incorporation of Sb_2O_3, SnO_2 and P_2O_5 in Ce-doped borosilicate glasses was executed, focusing on the structure, optical properties, luminescence, and scintillation.

1. Experimental procedures

The glass compositions were based on the SiO_2-B_2O_3-Na_2O-MgO-Ce_2O_3-Sb_2O_3/SnO_2/P_2O_5 system and designed using the proprietary software Reformix 2.0 (LaMaV-UFSCar, Brazil) and the Sciglass® database (ITC Inc.). The following analytical grade oxides and carbonates were used as precursors: high-purity quartz powder (99.99%, SiO_2, Vitrovita, Brazil), B_2O_3 (ESPI Metals, USA), Na_2CO_3 (99.5%, Vetec, Brazil), MgO (96%, Synth, Brazil), CeO_2 (99%, Vetec, Brazil), Sb_2O_3 (Fluka, Germany), SnO_2 (99.9% Riedel-de Haën, Germany), P_2O_5 (98%, Sigma Aldrich, UK). The nominal composition of the glasses is given in Table 1. The proper mixtures of these reagents were homogenized in a planetary ball mill (Fritsch Pulverisette 5) at 300 rpm for 12 min using a silicon nitride jar and eight 20 mm-diameter balls. The glasses were melted in an electrical furnace at atmospheric pressure at 1140 °C for 4 h in a platinum crucible. The melts were crushed, ball-milled using the same experimental conditions as before, and re-melted. They were re-melted over a total of two re-melting procedures to ensure homogeneity. Finally, the melts were poured on a stainless steel plate, pressed with a stainless steel plaque and annealed at 520 °C for 2 h. Since glass

* Corresponding author. Department of Materials Science and Engineering, Clemson University, Clemson, SC, USA.
E-mail address: luiz@clemson.edu (L.G. Jacobsohn).

https://doi.org/10.1016/j.optmat.2020.109847
Received 24 July 2019; Received in revised form 19 March 2020; Accepted 21 March 2020
Available online 31 March 2020

fabrication was executed without atmospheric control, partial conversion of Ce^{3+} to Ce^{4+} was expected to occur (see, *e.g.*, Refs. [21,22]). The surface of both sides of glass slabs were polished using a diamond solution for optical absorption measurements.

Specific density measurements were executed through the application of Archimedes' principle. The weight of each sample was determined both immersed in air (W_{air}) and in water (W_{water}), and the specific density calculated according to: $\rho = W_{air}/(W_{air} - W_{water})$ taking the density of water to be 1 g/cm^3. Three sets of measurements were done for each sample yielding a typical variation of the mass values with 1% standard deviation. The index of refraction was measured using a Carl Zeiss Jena refractometer Pulfrich-refraktometer PR2 at 546,1 nm after thorough polishing and cleaning of the glasses. The index of refraction was also estimated using the Gladstone-Dale relation [23,24] with the experimentally-determined density values as input.

Raman scattering spectroscopy was executed with a Horiba LabRAM HR Evolution Raman microscope equipped with an 800 mm focal length spectrograph and a cooled (−60 °C) back-illuminated deep-depleted 1024 × 256 pixels CCD detector using a 100 mW 532 nm laser with no attenuation, a 5x magnification objective, and 1800 groves/mm diffraction gratings. Spectra corresponded to the accumulation of five 15 s long scans. Each spectrum was corrected by the pre-recorded instrument-specific response to a calibrated white light source, namely the intensity correction system (ICS).

Optical absorption spectra were collected using a PerkinElmer Lambda 900 UV/Vis/NIR spectrometer.

Photoluminescence emission (PL) and excitation (PLE) measurements were executed using an Edinburgh Instruments FLS-1000 spectrofluorometer equipped with a 450 W Xe lamp and dual monochromators for emission and excitation. Excitation spectra were obtained within 240–360 nm and emission within 280/340-650 nm, depending on the sample, with excitation and emission bandwidths fixed at 0.4 nm. The number of detected photons was automatically corrected by the instrument's software for the background and spectral differences in excitation intensity and detection sensitivity.

Fluorescence lifetime was executed with an Edinburgh Instruments FLS-1000 spectrofluorometer using picosecond pulsed LEDs EPLED-310 emitting at 317.0 nm (9.6 nm FWHM bandwidth, 915.6 ps pulse width at 10 MHz; glass #3) and EPLED-330 emitting at 333.8 nm (9.3 nm FWHM bandwidth, 789.3 ps pulse width at 10 MHz; glasses # 1 and 2), depending on the position of the excitation band of the glass. A 2 nm bandwidth was used for detection with the monitoring wavelength being within 368–382 nm, while EPLED repetition rate was fixed at 0.5 MHz.

Radioluminescence (RL) measurements were executed using a customer-designed Freiberg Instruments Lexsyg Research spectrofluorometer equipped with a Varian Medical Systems VF-50J X-ray tube with a tungsten target coupled with an ionization chamber for irradiation dose monitoring. The light emitted by the sample was collected by a lens and converged into an optical fiber connected to an Andor Technology Shamrock 163 spectrograph coupled to an Andor Technology DU920P-BU Newton CCD camera. RL measurements were executed under continuous X-ray irradiation (40 kV, 1 mA) at room temperature (RT). Powders filled *ca.* 8 mm diameter 1 mm deep cups thus allowing for relative RL intensity comparison between different samples. The reproducibility of RL integrated intensities was within 8%. Results were not corrected for the spectral sensitivity of the system.

Thermoluminescence (TL) measurements were executed with a Freiberg Instruments Lexsyg Research spectrofluorometer equipped with a Hamamatsu H7360-2 photomultiplier tube using the following procedure: 1) TL readout up to 450 °C with a 1 °C/s heating rate and a 1 s integration time followed by cooling down to RT, 2) heating up to 450 °C and keeping the sample at 450 °C for 300 s to clean all traps, followed to cooling down to RT, 3) TL readout like in step 1, 4) X-ray irradiation (40 kV, 1 mA) for 100 s at RT, and 5) TL readout like in step 1. TL results presented in this work correspond to the last TL readout normalized by the total mass, *i.e.*, powder and cup, that was within 401.9 and 407.5 mg (for reference, the average of the mass of ten different cups was 375.5 mg).

2. Results and discussion

The Raman spectra of the glasses were similar and presented three groups of bands within about 230–850 cm^{-1}, 850-1250 cm^{-1}, and 1250-1600 cm^{-1} (Fig. 1). These bands are originated from the vibrations of the silicate and borate structural units. The small amount of P_2O_5 in glass #3 is not expected to yield active vibrational modes. It is known that the incorporation of alkali oxides in borate glasses alters the atomic network by disrupting boroxol rings and causing the appearance of a Raman peak at 765-775 cm^{-1} at the expense of the 805-810 cm^{-1} peak [25]. In fact, in both binary alkali borate and ternary alkali borosilicate glasses, the 805-810 cm^{-1} band was reported to disappear for high alkali

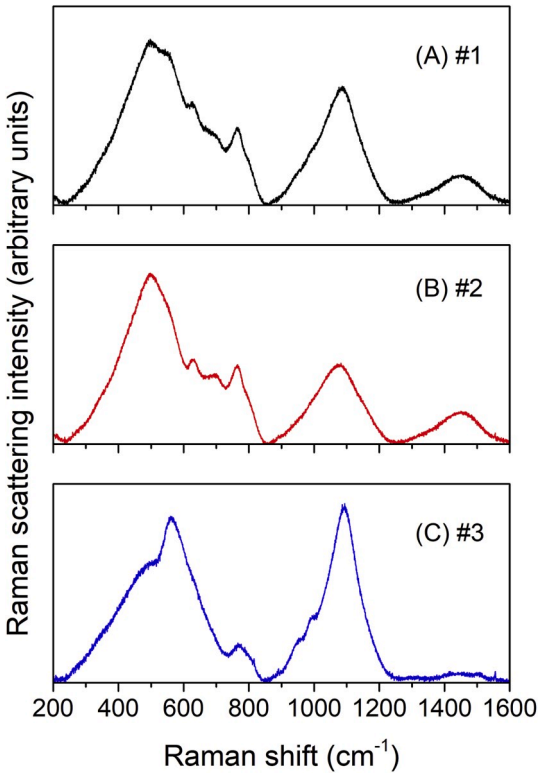

Fig. 1. Raman spectra of: A) glass #1, B) glass #2, and C) glass #3.

Table 1
Glass label, chemical composition, density, experimental index of refraction n, and calculated index of refraction using the Gladstone-Dale relation, n_{GD}.

Glass #	Molar fraction (%)								Density (g/cm^3)	n	n_{GD}
	SiO_2	B_2O_3	Na_2O	MgO	CeO_2	Sb_2O_3	SnO_2	P_2O_5			
1	47	28	14	10.8	0.1	0.1	-	-	2.6	1.528	1.53
2	47	28	14	10.8	0.1	-	0.1	-	2.4	1.525	1.50
3	47	28	14	10.8	0.1	-	-	0.1	2.4	1.526	1.51

concentrations [26–28]. In binary alkali borate glasses, it was shown that the incorporation of low concentrations of an alkali metal occurs by inducing the conversion of the coordination of boron from three to four, *i.e.*, the formation of BO_4^- units with an adjacent alkali ion for charge compensation. For higher alkali concentrations, charge compensation is achieved through the formation of non-bridging oxygen (NBO) adjacent to the alkali ion [27]. In ternary sodium borosilicate glasses with Na_2O/B_2O_3 ratios less than 1 (in this work, $Na_2O/B_2O_3 = 0.5$), it was shown that the majority of Na^+ ions are bonded to borate units, *i.e.*, they cause conversion of boron from coordination three to four while causing relatively few Si-O$^-$ non-bridging units. In ternary sodium borosilicate glasses, the Raman band within 450–550 cm^{-1} was ascribed to bending or rocking of Si-O-Si and Si-O-B bonds composing the three-dimensional network, *i.e.*, the incorporation of borate groups, BO_4 and BO_3 units into the silica network, the band within 620–635 cm^{-1} to a vibration of the metaborate ring, the band within 765–775 cm^{-1} to vibrations of six-membered borate rings with one or two BO_4 units, the band within 805–810 cm^{-1} to a symmetric vibration of the boroxol ring, the band within 950–975 cm^{-1} to the symmetric stretching of the non-bridging bonds of SiO_3 chain units (*i.e.*, Q^2 units), the band within 1050–1100 cm^{-1} to the stretching of the non-bridging bond of $SiO_{5/2}$ sheet units (*i.e.*, Q^3 units), and the band around 1460-1470 cm^{-1} to the stretching mode of B-O bonds [26 and references therein]. Also, Raman investigation of $xMgO{\cdot}yNa_2O{\cdot}B_2O_3$ glasses with $x + y = 1$ ascribed the band at 570 cm^{-1} to "loose" diborate units, at 760 cm^{-1} to six-membered borate rings with two BO_4 units, at 840 cm^{-1} to pyroborate units, and at 940 cm^{-1} to orthoborate units [29]. Accordingly, in this work, the band at about 497 cm^{-1} was ascribed to bending or rocking of Si-O-Si and Si-O-B bonds, at around 550 cm^{-1} to "loose" diborate units, at around 630 cm^{-1} to a vibration of the metaborate ring, at around 766 cm^{-1} to vibrations of six-membered borate rings with one or two BO_4 units, and the shoulder around 800 cm^{-1} to a symmetric vibration of the boroxol ring. The band at 975 cm^{-1} was ascribed to Q^2 units, the band at about 1083 cm^{-1} to Q^3 units, and the band at about 1452 cm^{-1} to the stretching mode of B-O bonds. The nature of a small band around 700 cm^{-1} could not be identified. The Raman spectra of glasses #1 and 2 were similar, while bands at 630 and 700 cm^{-1} were missing in the spectrum of glass #3. Also, the relative contribution of the band at about 1083 cm^{-1} in the spectrum of glass #3 was much higher than in the other glasses. These differences corresponded to the absence of metaborate rings and a higher content of Q^3 units in glass #3.

The density of the glasses was determined to be between 2.4 and 2.6 g/cm^3 (cf. Table 1) in agreement with the density values of other similar borosilicate glasses [15,30], and matching the density of commercial Ce-doped glass scintillators [31].

Table 1 shows the experimental and calculated values of the index of refraction. They were within a narrow range of values due to the small variation of density and chemical composition of the glasses, and in agreement with the measured values of the index of refraction of similar glasses [15,32]. While the Gladstone-Dale equation cannot account for dispersion, these results attested for its accuracy in estimating the index of refraction within the visible spectral range, where the relative error to the experimental values was inferior to 2%.

The optical absorption results are shown in Fig. 2 showing the glasses to be transparent up to ~315 nm, with glass #3 being the most ultraviolet transparent. The spectra presented a strong absorption band centered around ~302 nm ascribed to the $4f \rightarrow 5d$ transition of Ce^{3+} ions, in agreement with PLE results. The PLE and PL spectra are presented in Fig. 3. The PLE spectra were peaked around 320 nm, while displaying an asymmetric tail towards shorter wavelengths that was suggestive of the presence of additional excitation bands. The PLE spectrum of glass #3 presented another strong band centered at 270 nm. All PL spectra presented a single band centered within 360–370 nm, and excitation of glass #3 at 270 and 317 nm yielded the same emission spectrum. Glass #3 showed a considerably less self-absorption than the other glasses, as can be inferred by the small superposition between the

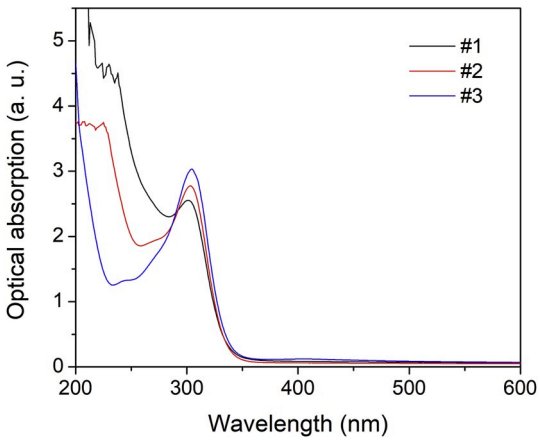

Fig. 2. Optical absorption of Ce-doped borosilicate glasses.

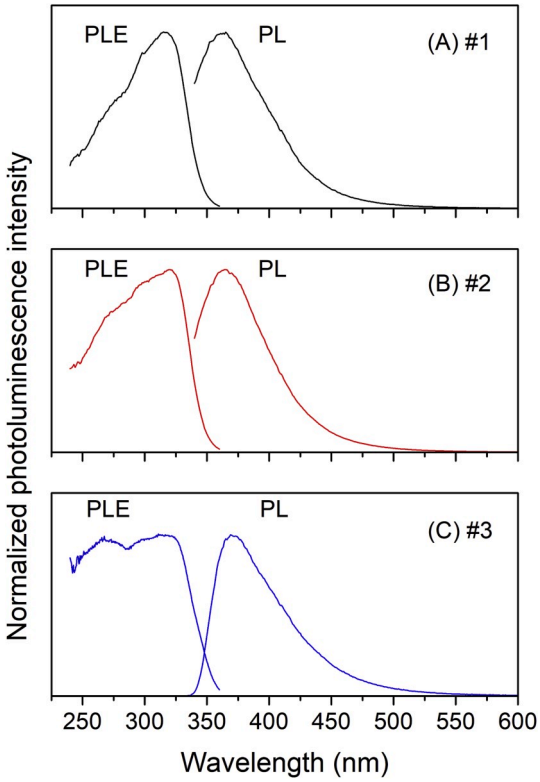

Fig. 3. Normalized PLE and PL spectra of A) glass #1: PLE monitored at 380 nm, and PL excited at 317 nm, B) glass #2: PLE monitored at 382 nm, and PL excited at 320 nm, and C) glass #3: PLE monitored at 368 nm, and PL excited at 262 nm.

excitation and emission spectra. The emission of the glasses reported in this work was in agreement with that of Ce-doped crystalline borosilicates $CaB_2O(Si_2O_7)$ at 343 nm, and $LaBO(SiO_4)$ at 377 nm [8 and references therein]. Moreover, Table 2 summarizes a literature review on the luminescence of Ce-doped borosilicate glasses where it is possible to check that the peak position of the excitation and emission bands found in this work are in good agreement with the reported results regardless the fabrication conditions [15,16,33–36].

Fluorescence lifetime results (circles) are presented in Fig. 4, together with best-fitting using two exponential functions (continuous lines). The decays were dominated (96–98%) by the fast lifetime component that ranged from 36 to 40 ns, in addition to the contribution of a longer lifetime component amounting to 145 ns for glass #1, 259 ns

Table 2
Summary of literature review on Ce-doped borosilicate glasses: glass composition, fabrication details, excitation and emission peak position, lifetime, and respective reference. The glass compositions presented here are indicative of the compositional range used in the original work. See references for details. RT = room temperature; NA = not available.

Glass composition	Fabrication details	Excitation Peak (nm)	Emission Peak (nm)	Lifetime (ns)	Ref.
$70B_2O_3$·(8–14.5)SiO_2·(0–20.8)Li_2O·1Al_2O_3·(0-20)Na_2O·(0.2–5) Ce_2O_3	Melting at 1000 °C in air Poured on graphite at RT	NA	341–353 372–432	NA	15
$20SiO_2$·(28-38)B_2O_3·15BaF_2·(10-20)Lu_2O_3·(10-20)Gd_2O_3·2CeF_3	Melting at 1400 °C in 95/5 N_2:H_2 Poured on heated stainless steel	*ca.* 260, 320	385	33–41	16
40Li_2O·yB_2O_3·(60-y)SiO_2 (0 ≤ y ≤ 40) + xCe in excess (0.1 ≤ x ≤ 2)	Melting at 1000 °C in Ar Poured on 200 °C stainless steel	*ca.* 323-345	*ca.* 363-394	37–45	33
15CaO·55B_2O_3·30SiO_2 +0.04 mol% CeO_2	Melting at 1500 °C in air Poured on 400 °C stainless steel	319	392	41	34
15SiO_2·30B_2O_3·25Al_2O_3·30Gd_2O_3 +1 wt% CeO_2	Melting at 1580 °C in CO Poured on heated stainless steel	*ca.* 350	410	40 (90%) + 136 (10%)	35
30SiO_2·25B_2O_3·30Gd_2O_3·15BaO +5 wt% CeO_2	Melting at 1350 °C in N_2 Poured at 1200 °C	360	450	21-31 + 64-74	36

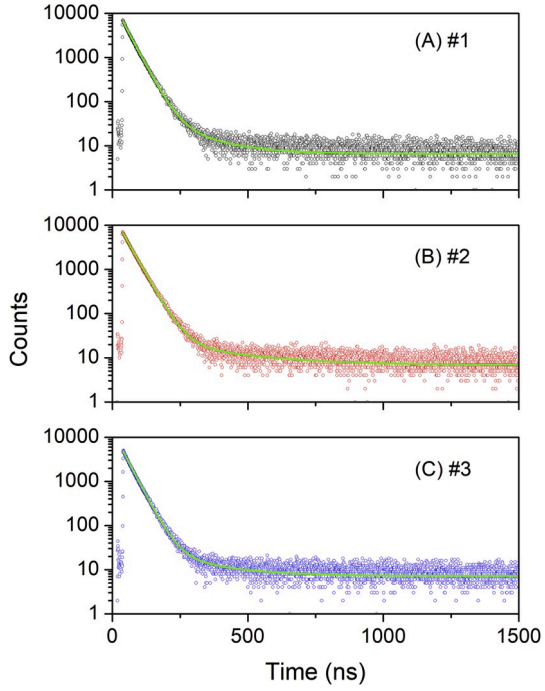

Fig. 4. Fluorescence decay of Ce-doped borosilicate glasses (circles) together with best-fit using two exponential functions (continuous lines) of: A) glass #1, B) glass #2, and C) glass #3.

for glass #2, and 181 ns for glass #3. The fast decay was ascribed to Ce^{3+} ions, and while the origin of the long lifetime was not known, it was believed to be originated from electrons that are thermally released from shallow traps and radiatively recombine at Ce^{3+} sites, in agreement with a small contribution of a few % to the temporal decay and strong TL signal at relatively low temperatures, as discussed below. These results were consistent with previous reports on Ce-doped phosphate and borosilicate glasses [33,35,37].

TL results of the glass powders are presented in Fig. 5 together with the TL response of an empty cup. Overall, the TL response of the glasses corresponded to broad glow peaks in agreement with the disordered nature of glass structures, with a significant contribution at relatively low temperatures. The steep increase for temperatures above about 350 °C corresponded to the blackbody response of the system, as demonstrated by the measurement of the empty cup. These data were analyzed in terms of the integral TL signal, with glass #3 presenting an integrated TL response 12x and glass #2 8x that of glass #1.

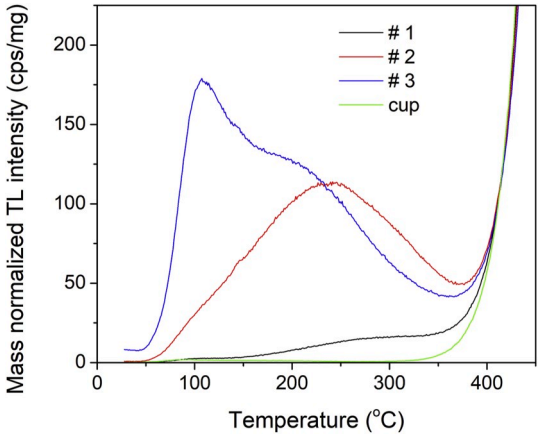

Fig. 5. TL glow curves of Ce-doped borosilicate glasses, together with the TL response of an empty cup.

RL results are presented in Fig. 6. The spectra are dominated by a broad band centered at 372 nm for glass #1, 369 nm for glass #2, and 373 nm for glass #3, depending on the glass composition, in agreement with PL results. The weaker bands around 700 nm and within *ca.* 470–640 nm were ascribed to Fe^{3+} impurity, in accord with Fe^{3+} emission band in quartz at 709 nm [38], and to Eu^{3+}, respectively. These impurities could not be detected by energy dispersive X-ray spectroscopy (EDX) measurements, showing them to be trace contamination.

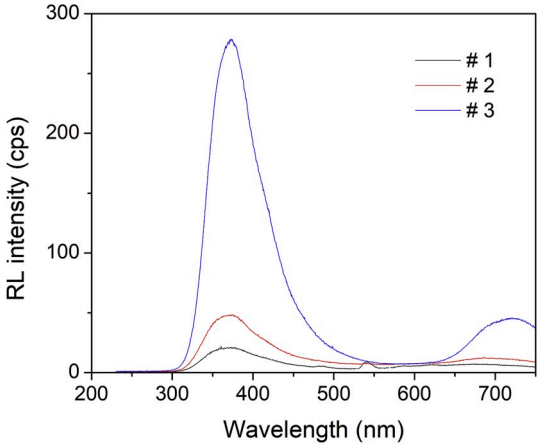

Fig. 6. RL spectra of Ce-doped borosilicate glasses.

Their small concentration was not expected to cause any significant effect on the luminescence of Ce^{3+}. The dependence of Ce^{3+} luminescence on the host is due to the lack of shielding of the 5*d* orbital to outer electrons making the $5d \rightarrow 4f$ transition sensitive to the physical arrangement and chemical nature of the surrounding atoms [8–12]. The RL spectra were integrated within 275–470 nm, yielding the relative luminosity of the glasses. Glass #3 was 5.2x brighter than glass #2 and 11.6x brighter than glass #1, while glass #2 was 2.2x brighter than glass #1, in agreement with the optical absorption results and reduced self-absorption presented by glass #3.

3. Conclusions

We investigated Ce-doped borosilicate glasses which yielded insights into the effects of the addition of Sb_2O_3, SnO_2 and P_2O_5 on their optical and luminescent properties. The incorporation of P_2O_5 was advantageous over Sb_2O_3 and SnO_2, leading to superior ultraviolet transparency, reduced self-absorption of Ce^{3+} emission, and brighter scintillation under X-ray irradiation.

Author agreement

This document serves to confirm that the work described in the manuscript has not been published before, it is not under consideration for publication anywhere else, and its publication has been approved by all co-authors and the responsible authorities at the institutions where the work was carried out.

Declaration of competing interest

The authors declare that they have no known competing financial interests or personal relationships that could have appeared to influence the work reported in this paper.

CRediT authorship contribution statement

Linyu Pan: Formal analysis, Investigation, Writing - review & editing. **Juliana K.M.F. Daguano:** Investigation, Resources, Writing - review & editing. **Neilo M. Trindade:** Investigation, Writing - review & editing. **Mayara Cerruti:** Investigation. **Edgar D. Zanotto:** Conceptualization, Methodology, Resources, Writing - review & editing, Project administration, Funding acquisition. **Luiz G. Jacobsohn:** Conceptualization, Methodology, Formal analysis, Investigation, Resources, Writing - original draft, Writing - review & editing, Project administration, Funding acquisition.

Acknowledgements

This material is based upon work supported by the National Science Foundation under Grant No. 1653016. N.M. Trindade is grateful to the São Paulo Research Foundation (FAPESP) Grants #2017/11663-1 and #2019/05915-3. E.D. Zanotto is grateful to the São Paulo Research Foundation (FAPESP) Grant #2013/007793-6 for the partial support of this research.

References

[1] C. Grescovich, S. Duclos, Annu. Rev. Mater. Sci. 27 (1997) 69.
[2] C.W.E. van Eijk, Phys. Med. Biol. 47 (2002) R85.
[3] G.C. Tyrrell, Nucl. Instrum. Methods Phys. Res. A 546 (2005) 180.
[4] M. Nikl, Meas. Sci. Technol. 17 (2006) R37.
[5] L.A. Boatner, J.S. Neal, J.A. Kolopus, J.O. Ramey, H. Akkurt, Nucl. Instrum. Methods Phys. Res. A 709 (2013) 95.
[6] T. Yanagida, Y. Fujimoto, S. Kurosawa, K. Kamada, H. Takahashi, Y. Fukazawa, M. Nikl, V. Chani, Jap. J. Appl. Phys. 52 (2013), 076401.
[7] C. Dujardin, E. Auffray, E. Bourret, P. Dorenbos, P. Lecoq, M. Nikl, A.N. Vasil'ev, A. Yoshikawa, R. Zhu, IEEE Trans. Nucl. Sci. 65 (2018) 1977.
[8] P. Dorenbos, J. Lumin. 91 (2000) 155.
[9] P. Dorenbos, Phys. Rev. B 62 (2000) 15640.
[10] P. Dorenbos, Phys. Rev. B 62 (2000) 15650.
[11] P. Dorenbos, Phys. Rev. B 64 (2000), 125117.
[12] P. Dorenbos, J. Lumin. 99 (2002) 283.
[13] M.W. Kielty, L. Pan, M.A. Dettmann, V. Herrig, U. Akgun, L.G. Jacobsohn, J. Mater. Sci. Mater. Electron. 30 (2019) 16774.
[14] I.J. Tillman, M.A. Dettman, V.V. Herrig, Z.L. Thune, A.J. Zieser, S.F. Michalek, M. O. Been, M.M. Martinez-Szewczyk, H.J. Koster, C.J. Wilkinson, M.W. Kielty, L. G. Jacobsohn, U. Akgun, Opt. Mater. 68 (2017) 58.
[15] M.W. Kielty, M. Dettmann, V. Herrig, M.G. Chapman, M.R. Marchewka, A. A. Trofimov, U. Akgun, L.G. Jacobsohn, J. Non-Cryst. Sol. 471 (2017) 357.
[16] Q. Wang, B. Yang, Y. Zhang, H. Xia, T. Zhao, H. Jiang, J. Alloys Compd. 581 (2013) 801.
[17] J.L. Rygel, C.G. Pantano, J. Non-Cryst. Solids 355 (2009) 2622.
[18] J. Bei, G. Qian, X. Liang, S. Yuan, Y. Yang, G. Chen, Mater. Res. Bull. 42 (2007) 1195.
[19] M. Rodová, A. Cihlar, K. Knizek, K. Nitsch, N. Solovieva, Radiat. Meas. 38 (2004) 489.
[20] J. Jiang, G. Zhang, M. Poulain, J. Alloys Compd. 275–277 (1998) 733.
[21] A. Herrmann, H.A. Othman, A.A. Assadi, M. Tiegel, S. Kuhn, C. Rüssel, Opt. Mater. Express 5 (2015) 720.
[22] M.R. Cicconi, D.R. Neuville, W. Blanc, J.-F. Lupi, M. Vermillac, D. de Ligny, J. Non-Cryst. Solids 475 (2017) 85.
[23] J.A. Mandarino, Can. Mineral. 14 (1976) 498.
[24] J.A. Mandarino, Can. Mineral. 19 (1981) 441.
[25] W.L. Konijnendijk, J.M. Stevels, J. Non-Cryst. Solids 18 (1975) 307.
[26] T. Furukawa, W.B. White, J. Mater. Sci. 16 (1981) 2689.
[27] B.P. Dwivedi, B.N. Khanna, J. Phys. Chem. Solid. 56 (1995) 39.
[28] E.I. Kamitsos, M.A. Karakassides, G.D. Chryssikos, J. Phys. Chem. 90 (1986) 4528.
[29] E.I. Kamitsos, A. Karakassides, G.D. Chryssikos, J. Phys. Chem. 91 (1987) 1073.
[30] M. Barlet, A. Kerrache, J. Delaye, C.L. Rountree, J. Non-Cryst. Sol. 382 (2013) 32.
[31] http://www.crystals.saint-gobain.com/products/lithium-glass-scintillators. http://www.scintacor.com/wp-content/uploads/2015/09/GlassScintillators.pdf.
[32] https://www.schott.com/advanced_optics/english/abbe_datasheets/schott-datasheet-all-english.pdf.
[33] H. Masai, T. Yanagida, Opt. Mater. Express 5 (2015) 1851.
[34] T.-S. Lv, X.-H. Xu, X. Yua, H.-L. Yu, D.-J. Wang, D.-C. Zhou, J.-B. Qiu, J. Non-Cryst. Sol. 385 (2014) 163.
[35] W. Chewpraditkul, X. He, D. Chen, Y. Shen, Q. Sheng, B. Yu, M. Nikl, R. Kucerkova, A. Beitlerova, C. Wanarak, A. Phunpueok, Phys. Status Solidi 208 (2011) 2830.
[36] C. Jiang, P. Deng, J. Zhang, F. Gan, Phys. Lett. 323 (2004) 323.
[37] D. Wisniewski, L.A. Boatner, J.O. Ramey, M. Wisniewska, J.S. Neal, G. E. Jellison Jr., IEEE Trans. Nucl. Sci. 55 (2008) 3692.
[38] J. Götze, M. Plötze, D. Habermann, Mineral. Petrol. 71 (2001) 225.